3D CT Non-rigid Registration for Deformation Evaluation: Study of Breath-hold Reproducibility for Radiotherapy Treatment

Vlad Boldea[1], David Sarrut[1,2], Chantal Ginestet[2] and Christian Carrie[2]

[1] LIRIS, Université Lumière Lyon 2, 5 Av. P. Mendès-France, 69676 Bron, France
[2] Radiotherapy Dpt, Centre Léon Bérard, 28 rue Laennec, 69353 Lyon, France

Abstract. Breath holding (BH) can be an effective method to immobilize organs during radiotherapy treatment of lung cancer. As shown in our previous study, non-rigid registration methods applied on 3D CT scans acquired in BH can be used to evaluate the breath holding reproducibility by providing 3D displacement vector fields in order to adapt internal margins for each patient. In this work we propose to compare two non-rigid registration schemes (with Gaussian and linear-elastic regularization) and to analyze resulting vector fields by several operators (deformation consistency, volume dilatation) in order to provide automated way to detect abnormal situations (algorithm failure or anatomical discrepancies such as atelectasis).

1 Medical context

The main challenge for lung cancer radiotherapy is to provide prescribed doses to the tumor while sparing surrounding normal tissues. This is a challenging task because of organs and tumors motions. Incorporating organ deformation can be achieved with several approaches : adapting internal margins (as defined in ICRU Report 62), synchronizing radiation delivery with breathing (but it requires invasive internal markers or depend on an hypothetical correlation between external and internal movements [1]), or holding patient breath.

We are involved in a project consisting in immobilizing the organs and tumors by active breath-holding (BH). The goal is to study internal lung deformation between 3D CT scans acquired at a same level of the breathing cycle with Active Breath Control (ABC) device [2]. In previous work [3] we proposed the use of non-rigid registration method. In this work, we have two goals : compare two regularization approaches (gaussian and linear elastic) and provide automated methods to evaluate resulting vector fields. However, we do not dispose of gold standard and we cannot use expert validation because we are requiring automated tools. So we studied a set of measures (deformation consistency, lung volume and surface comparisons, volume dilatation) in order to detect abnormalities or algorithm failures automatically.

2 Dense Non-rigid Registration

2.1 Introduction

Non rigid registration algorithms were used for multiple purposes on monomodal and multimodal images registration, especially for brain and heart. At our knowledge there are a few works for 3D non rigid registration of thorax CT scans [4, 5]. Dense non-rigid intensity based registration algorithm can be expressed as a a criterion minimization. The criterion is a trade-off between two energies : similarity energy (E_1) and regularization energy (E_2). The similarity energy E_1 quantifies the images alignment quality. The regularization energy E_2 constrains the deformation field to have some spacial coherence. Equation 1 summarizes the general formulation. U denotes a deformation field, $\tilde{U}$ denotes the final solution, β $(0 \leq \beta \leq 1)$ denotes a tradeoff factor between the two energies.

$$\tilde{U} = \arg\min_{U}(E(U)) \quad ; \quad E(U)) = (1-\beta)E_1(U) + \beta E_2(U) \tag{1}$$

2.2 Current and previous work

In previous work [3], we focused on the "demons" algorithm proposed by Thirion and modified by Cachier [6, 7]. Due to a Gaussian regularization of the vector field, this method can be viewed as an elastic-like algorithm [7] or an homogenous isotropic diffusion. First results allowed us to evaluate BH reproducibility from CT deformation.

We implemented a second method using the "demons" forces for estimating points correspondence and using the linearized elasticity operator for regularization [8, 9]. The general form of this operator is inspired from the equilibrium equation 2 under the hypothesis of small displacements where λ and μ are the Lamé coefficients and F are the applied volume forces. $F = 0$ if deformation is due to surface forces only.

$$(\lambda+\mu)\nabla(\nabla \cdot U) + \mu \cdot \triangle U = -F \tag{2}$$

A solution to the minimization equation 1 can be found by solving the equivalent Euler equations [9] : $\nabla E(\tilde{U}) = 0$. We considered the Euler explicit equation 3 for an iterative implementation of the algorithm. κ $(\kappa > 0)$ denotes the descent step size, $\boldsymbol{x}$ denotes an image point, ∇ the gradient operator and i the iteration index.

$$U_i(\boldsymbol{x}) = U_{i-1}(\boldsymbol{x}) + \kappa((1-\beta)\nabla E_1(U_{i-1}(\boldsymbol{x})) + \beta\nabla E_2(U_{i-1}(\boldsymbol{x}))) \tag{3}$$

[7] demonstrates that the "demons" forces are closed to a second order gradient descent of an SSD criterion under the hypothesis of small correction field. Under this assumption we used the "demons" forces (eq 4) as gradient of the similarity criterion. I and J denote the images, Id denotes the identity matrix, the α $(\alpha > 0)$ parameter introduced by [7] limits the displacement vector for small gradients: the norm is bounded by $1/(2\alpha)$.

$$\nabla E_1(U_{i-1}(\boldsymbol{x})) = u_i(\boldsymbol{x}) = \frac{I(\boldsymbol{x}) - J(Id + U_{i-1}(\boldsymbol{x}))}{\| \nabla I \|^2 + \alpha^2(I(\boldsymbol{x}) - J(Id + U_{i-1}(\boldsymbol{x})))^2}\nabla I \tag{4}$$

[10] shows that gaussian regularization is related (under some assumptions) to linear elastic filter. Linear elastic regularization allows to take into account cross-effects while Gaussian smoothing does not [11]. The gradient of the regularization energy is computed with linearized elasticity operator summarized by the equation 5. We used spatial difference scheme [9] for the evaluation of differential operators. Instead of using Lamé coefficients, [9] introduces ξ $(0 < \xi \leq 1)$ to have a diffusion-like method.

$$\nabla E_2(U_{i-1}(\boldsymbol{x})) = (1-\xi)\nabla(\nabla \cdot U_{i-1}(\boldsymbol{x})) + \xi \triangle U_{i-1}(\boldsymbol{x}) \tag{5}$$

We thus have two different ways to compute vector fields : the first method M_1 is the "demons" algorithm with Gaussian regularization and the second method M_2 with linear elastic regularization.

3 Materials and methods

3.1 Materials

Eight patients were involved in this study. For each, 3D CT scans are acquired in BH at a determined level of the breathing cycle (about 70% of the vital capacity). The scans have $5\,mm$ inter-plane and $0.9\,mm$ intra-plane resolution, leading to $512 \times 512 \times 65$ image resolution. As mentioned in our previous work it is important to encode voxel values in 16 bits in order to keep the full range of Hounsfield units[1] related to density information.

3.2 Methods

Non-rigid registration parameters Vector fields were estimated at a resolution of $256 \times 256 \times 65$ which corresponds to $1.9\,mm$ in intra-plane and $5\,mm$ inter-plane resolution. For M_1, we used $\alpha \in [0.5, 0.65]$ which is equivalent to a maximum estimated vector displacement of $[0.77, 1]$ voxel by iteration, 150 iterations and a Gaussian variance of 1.0. For M_2, we used the same α value. A good empirical convergence was obtained for $\kappa = 0.1$ (smaller values leaded to slower convergence and values larger than 0.3 leaded to divergence). Trade-off parameter β was set to 0.5. ξ was set to 0.6 to slightly privilege the Laplacian operator. Convergence for the algorithm was obtained with at least 700 iterations.

Transitivity error We propose to evaluate the consistency of the vector field by evaluating the transitivity as suggested in [12]. Scheme 1 illustrates deformation evaluation between images. The three acquisitions for each patient are denoted by A, B, C, each being alternatively reference and deformed image. U_{XZ} denotes the deformation field estimated between X (reference) and Z (deformed), with X,Z $\in$ {A,B,C}. Computed deformation between two images may be expressed

[1] Hounsfield density values for humain body are approximatively from -1000 to 4000. 0 corresponds to water and -1000 to air.

using the third image as intermediate result of the final transformation. The deformation field from X to Z can be written by transitivity $U'_{XZ} = U_{XY} \circ U_{YZ}$, with Y the third image. We computed the mean, $\sigma_{er}(X, Z)$, and the standard deviation, $\mu_{er}(X, Z)$ of the norm of the difference between U'_{XZ} and U_{XZ} for points belonging to the lung. Lung volume and lung surface points are extracted by thresholding and morphological operations [3].

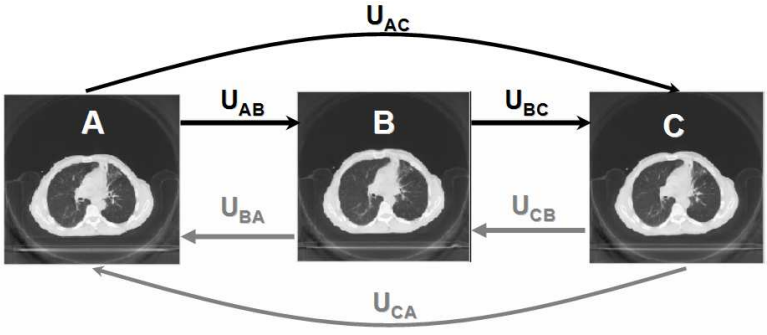

Fig. 1. Deformation field computation scheme : each acquisition (A, B and C) is alternatively reference and object image.

Pure deformation A misalignment may occur between two scan acquisitions X and Y, due to patient setup error. This setup error can be expressed as a global rigid transformation R_{XY}. We applied a 3D rigid registration algorithm by privileging rigid bonny structures. Pure deformation, denoted by U^p is obtained by subtracting this global rigid deformation from the computed vector field by non-rigid registration: $U^p_{XY} = U_{XY} - R_{XY}$.

Volume dilatation evaluation Continuum mechanics is a source of inspiration for medical image registration. Image X may be considered as deformed (reference) body and Y image as deformable body. Each image voxel may be viewed as an elementary volume element. We considered here operators which are related to volume variation in order to be able to compare with lung volume measures done by segmentation. The divergence of the deformation function was proposed by [13]: $div(Id + U^p_{XY}) = trace(Id + \nabla U^p_{XY})$. Divergence measures the difference between inflow and outflow through an elementary volume element. Negative divergence value means local contraction while positive value means local dilatation. Divergence is computed with 3D Gaussian recursive filter. To differentiate contraction from dilatation, we calculated the change of volume per unit volume of each voxel to divergence value : $\text{abs}(V_1(\boldsymbol{x}) - V_0(\boldsymbol{x}))/V_0(\boldsymbol{x})$, with $V_0(\boldsymbol{x})$ the initial volume of $\boldsymbol{x}$ and $V_1(\boldsymbol{x})$ volume after deformation. $V_1(\boldsymbol{x})$ is computed as follows. The deformation tensor for each point $\nabla U^p_{XY}(\boldsymbol{x})$ can be decomposed in a symmetric part, denoted by $V_{XY}(\boldsymbol{x})$ (local pure deformation) and an asymmetric part, denoted by $W_{XY}(\boldsymbol{x})$ (local rotation). We can write $\nabla U^p_{XY}(\boldsymbol{x}) = V_{XY}(\boldsymbol{x}) + W_{XY}(\boldsymbol{x})$, with $V_{XY}(\boldsymbol{x}) = \frac{1}{2}(\nabla U^p_{XY}(\boldsymbol{x}) + (\nabla U^p_{XY}(\boldsymbol{x}))^T)$

and $W_{XY}(\boldsymbol{x}) = \frac{1}{2}(\nabla U^p_{XY}(\boldsymbol{x}) - (\nabla U^p_{XY}(\boldsymbol{x}))^T)$. The local volume change is thus $V_1(\boldsymbol{x}) = det(V_{XY}(\boldsymbol{x}))$. Total variation of lung volume due to deformation is computed with equation 6.

$$Vol_{change}(X) = \frac{1}{N} \sum_{\boldsymbol{x} \in \Omega_X} \text{sgn}(div(Id + U^p_{XY}(\boldsymbol{x}))) \frac{\text{abs}(V_1(\boldsymbol{x}) - V_0(\boldsymbol{x}))}{V_0(\boldsymbol{x})} \quad (6)$$

$$\text{with} \quad \text{sgn}(div(Id + U^p_{XY}(\boldsymbol{x}))) = \begin{cases} 1, & \text{if } div(Id + U^p_{XY}(\boldsymbol{x})) \geq 0 \\ -1, & \text{if } div(Id + U^p_{XY}(\boldsymbol{x})) < 0 \end{cases}$$

Jacobian of the deformation function measures the evolution of elementary volume $\boldsymbol{x}$ [14] : $J = Jac(Id + U^p_{XY}(\boldsymbol{x})) = V_1(\boldsymbol{x})/V_0(\boldsymbol{x})$. $J > 1$ corresponds to a local dilatation, $J < 1$ to a local contraction and $J = 1$ to no volume change. We have used this operator to evaluate the coherence of the transformation: negative value of the jacobian means that the deformation is locally non-invertible.

4 Results

For each patient we have performed 12 non-rigid registrations (each of the 3 acquisitions is alternatively the reference and the floating image, 2 methods) leading to 96 deformation fields. Stopping criterion was chosen with respect to mean of absolute intensity difference. In a related study done in collaboration with physicians (starting in [3]), patients were classified into two categories: for five patients breath hold was considered as effective (group I) and for three other patients (group II), we detected abnormal behavior due to atelectasis and emphysema. Average displacement of lung points for the first group was $2,7\,mm$ ($1.7\,mm$) and average displacement of lung surface points was $2,5\,mm$ ($1.7\,mm$). In second group, average displacements are $5.3\,mm$ ($3.6\,mm$) for volume points and a $5.2\,mm$ ($4\,mm$) for surface points. Results were similar for the 2 methods.

In the following, due to the limited space, we only present results for two patients, one in each category. Figure 2 illustrates the convergence of the algorithm with both methods for two patients according to the algorithm iteration. The two first upper curves are related to the patient in group II and the two others curves to the patient in group I. Table 1 shows the transitivity error (μ_{er} and σ_{er}) of the computed vector fields with M_1 and M_2 for the two patients. Values are given in mm. Left table 2 shows the percentage of lung volume change between acquisitions computed from lung masks (first column) and computed with previously described local dilatation operators (2 other columns). Positive values correspond to volume increases and negative values to volume decreases. Right table 2 shows the percentage of points with negative Jacobian for the two patients and the two methods.

5 Discussion and conclusion

Gaussian regularization leads to faster convergence (about 150 iterations) than linear elastic regularization (it requires a minimum of 700 iterations for patients

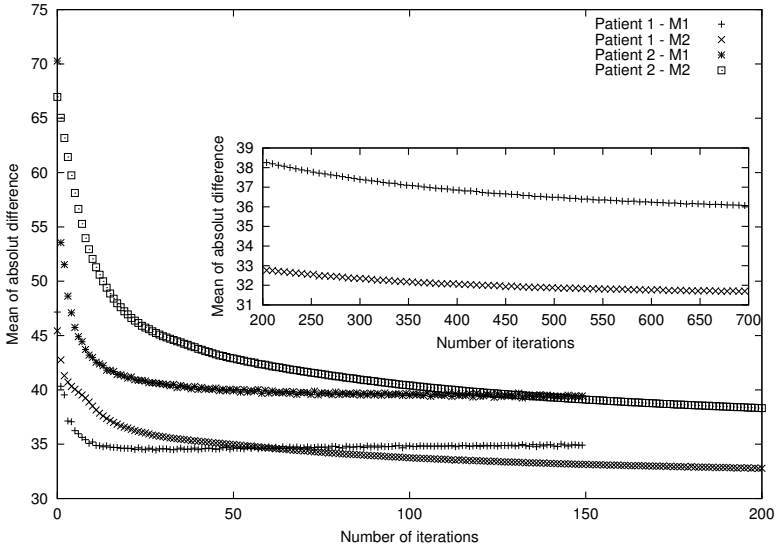

Fig. 2. Mean of intensity absolute differences between two registered images according to the algorithm iteration. The two upper curves show the convergence with both methods for the patient in group II and the two others show convergence for the patient in group I.

Table 1. Mean and standard deviation error of the deformation for the 2 methods and 2 patients according to the transitivity property

	M_1		M_2	
Deformation transitivity	Patient 1 $\mu_{er}(\sigma_{er})$	Patient 2 $\mu_{er}(\sigma_{er})$	Patient 1 $\mu_{er}(\sigma_{er})$	Patient 2 $\mu_{er}(\sigma_{er})$
A,B	1.7 (1.0)	2.8 (2.6)	2.1 (1.2)	2.4 (2.1)
A,C	1.6 (0.9)	2.9 (3.4)	2.1 (1.1)	2.2 (1.8)
B,A	1.9 (1.1)	2.7 (2.6)	1.7 (0.9)	2.2 (1.9)
B,C	1.7 (1.0)	2.6 (2.6)	2.1 (1.2)	2.2 (1.9)
C,A	1.7 (1.0)	3.7 (4.7)	3.8 (2.5)	4.2 (2.2)
C,B	1.9 (1.3)	2.8 (2.7)	1.8 (1.1)	2.3 (2.0)
Mean	1.8 (1.0)	2.9 (3.1)	2.3 (1.3)	2.6 (2.0)

of group I while and even more iterations are needed for group II with larger deformation).

We noticed that the transitivity error is relatively small (mean $1.8\,mm$) with patients from group I compared to group II (mean $2.9\,mm$). It suggests that such measure can help for abnormalities detection. Moreover, for patient transitivity analysis leads to slightly better results with M1 than with M2.

Table 2 compares a global measure of lung volume difference computed from segmentation with local lung volume changes computed from the vector fields in

Table 2. (Left table) Lung volume dilation for 3 images comparisons for 2 patients. Each column depicts the increasing volume (in %, computed from segmented lung) and the dilatation operators computed with the resulting vector field of the 2 algorithms. (Right table) Percentage of points with negative Jacobian computed on each vector fields for the 2 methods and the 2 patients (P1 and P2).

Dilat.	Patient 1 (%)			Patient 2 (%)		
	Vol.	M_1	M_2	Vol.	M_1	M_2
AB	3.9	3.3	2.8	-6.6	-6.5	-5.9
AC	4.1	3.6	3.3	5.6	4.4	4.2
BA	-3.9	-4.5	-3.7	6.6	4.8	4.3
BC	0.4	-1.2	-1.0	13.1	10.5	9.4
CA	-4.1	-5.0	-4.6	-5.6	-6.2	-5.8
CB	-0.4	-0.3	-0.4	-13.1	-12.2	-10.9

Jacob	M_1		M_2	
	P1 (%)	P2 (%)	P1 (%)	P2 (%)
AB	1.3	10.1	0.6	6.6
AC	2.1	5.5	0.7	2.7
BA	6.2	6.2	4.0	3.2
BC	3.4	5.6	1.7	2.4
CA	5.7	9.2	3.0	5.9
CB	1.4	16.7	0.6	12.3

order to detect incoherent situations. We first notice that the two analysis are very related : it suggests that the computed vector fields are coherent according to the observed volume change. Results are also related with the average displacements of the two patient groups : group I presents smaller displacements than group II. Moreover, M1 presents volume changes more closely related to those observed with M2. It suggests that more iterations are needed for M2. For patient 1, we observe for the BC case, a discrepancy between the globally and locally computed volume changes. It may be due to the final oscillations of the algorithms when approaching matching solution and to a difficult lung segmentation : the correction field estimated may be locally greater than the real deformation needed for perfect matching and thus object image is deformed more than needed. This phenomena was also observed by [15]. Hence, this information may be considered for evaluating the stop criterion.

The number of points with negative Jacobian can be a measure of the validity of the transformation. Deformation fields computed with M1 present a greater number of negative Jacobian points then with M2. We also noticed that a global lung contraction implies a bigger percentage of points with negative Jacobian. For patient 2, there is a very important volume change between acquisitions B and C but the number of Jacobian negative points in the dilatation case BC is more important than for the contraction CB.

In this work, we analyzed two non-rigid registration schemes to evaluate BH reproducibility and proposed several operators to help automatically evaluate the validity of resulting vector fields. This study will serve as basis to include in the non-rigid registration method an automated abnormalities detection process. Further works are on going in order to take into account the heterogeneity and anisotropic nature of lung deformation during respiration. In [16], Christensen jointly estimates forward and reverse transformation between images while constraining these transforms to be inverses of one other. We plan to follow a similar scheme by estimating the deformation field using the 3 acquisitions and constraining the transformation to be transitive. In this preliminarily work we do not manage to clearly define an abnormal situations detector operator, but

provide a set of indications which will be combined to evaluate the BH reproducibility.

Acknowledgement : This work was supported in part by Elekta Oncology Systems.

References

1. C. Ozhasoglu and MJ. Murphy. Issues in Respiratory Motion Compensation During External-beam Radiotherapy. *International Journal of Radiation Oncology Biology Physics*, 52(5):1389–99, 2002.
2. J.W. Wong, M.B. Sharpe, D.A. Jaffray, V.R Kini, J.M. Robertson, J.S. Stromberg, and A.A. Martinez. The Use of Active Breathing Control (ABC) to Reduce Margin for Breathing Motion. *Int. J. Radiat. Oncol. Biol. Phys.*, 44(4):911–919, July 1999.
3. V. Boldea, D. Sarrut, and S. Clippe. Lung Deformation Estimation with Non-rigid Registration for Radiotherapy Treatment. In *MICCAI'2003*, volume 2878, pages 770–777, Montreal (Canada), 2003. LNCS.
4. L. Fan, C.W. Chen, J.M. Reinhardt, and E.A. Hoffman. Evaluation and Application of 3d Lung Warping and Registration Model Using HRCT Images. In *SPIE Medical Imaging*, San Diego, CA, 2001.
5. L. Weruaga, J. Morales, L. Nunez, and R. Verdu. Estimating Volumetric Motion in Thorax with Parametric Matching Constraints. *IEEE T. Med. Im.*, 22(6):766–772, June 2003.
6. J.P. Thirion. Image Matching as a Diffusion Process: an Analogy with Maxwell's Demons. *Medical Image Analysis*, 2(3):243–260, 1998.
7. P. Cachier, X. Pennec, and N. Ayache. Fast Non-rigid Matching by Gradient Descent: Study and Improvements of the "Demons" Algorithm. Technical Report RR3706, INRIA, 1999.
8. P.G. Ciarlet. *Mathematical Elasticity*, volume 1. North Holland, Amsterdam, 1988.
9. G. Hermosillo. *Variational Methods for Multimodal Image Matching.* PhD thesis, Université de Nice Sophia-Antipolis, May 2002.
10. M. Bro-Nielsen. *Medical Image Registration and Surgery Simulation.* PhD thesis, Technical University of Denmark, 1996.
11. P. Cachier and N. Ayache. Regularization Methods in Non-rigid Registration: II. Isotropic Energies, Filters and Splines. Technical Report 4243, INRIA, 2001.
12. X. Pennec, C.R.G. Guttmann, and J.-P. Thirion. Feature-based Registration of Medical Images: Estimation and Validation of the Pose Accuracy. In *MICCAI'1998*, volume 1496 of *LNCS*, pages 1107–1114, Cambridge (USA), October 1998. Springer Verlag.
13. Jean-Philippe Thirion and Guillaume Calmon. Measuring Lesion Growth from 3D Medical Images. In *Non Rigid and Articulated Motion Workshop (NAM '97) in Conjunction with CVPR '97*, June 1997.
14. David Rey, Gérard Subsol, Hervé Delingette, and Nicholas Ayache. Automatic Detection and Segmentation of Evolving Processes in 3D Medical Images: Application to Multiple Sclerosis. *Medical Image Analysis*, 6(2):163–179, June 2002.
15. H.Helminen, J.Alakuijala, K. Pesola, and J.Laitinen. Comparision of Local External Force Functions for Non-rigid Registration of 3D Medical Images. In *MICCAI'2003*, volume 2879, pages 821–828, Montreal (Canada), 2003. LNCS.
16. G.E. Christensen and H.J. Johnson. Consistant image registration. *IEEE T. Med. Im.*, 20(7):568–582, 2001.